MATERIALS CHEMISTRY
FRONTIERS

RESEARCH ARTICLE

View Article Online
View Journal | View Issue

Cite this: *Mater. Chem. Front.*, 2023, **7**, 4092

Suppression and utilization of Kasha's rule: realizing the transformation from blue to near-infrared emission†

Mingchen Xie,‡[a] Jia-Heng Cai,‡[b] Guangyu Zhang,[c] Sinyeong Jung,[a] Dongfang Dong,[a] Zhao-Yang Zhang,[a] Dong-Ying Zhou,*[b] Liang-Sheng Liao[b] and Tao Li*[a]

Received 14th April 2023,
Accepted 22nd June 2023

DOI: 10.1039/d3qm00394a

rsc.li/frontiers-materials

Kasha's rule emphasizes that excitons should deexcite from the lowest excited state; indeed most luminous emitters follow this rule. However, little effort has been made to suppress and utilize Kasha's rule to realize variable emission from the perspective of modulating the molecular configuration. In this paper, phenoxazine–phenazine (POZ–PZ) is selected as the objective molecule that could exhibit dual emission (~420 nm visible mazarine and 780 nm weak NIR) in the solution state *via* the suppression of Kasha's rule through the vertical molecule configuration. Contrarily, POZ–PZ can exhibits NIR-only emission (peak at ~760 nm in the thin film state) *via* the utilization of Kasha's rule when it is doped into rigid matrixes. The visible chromatism range can reach up to ~340 nm. Based on the experimental results, we propose that the molecular configuration and intramolecular motion of POZ–PZ would be induced by the matrixes until the molecule arrives at a self-consistent state, further presenting the specific photophysical properties. Meanwhile, POZ–PZ is also employed as a guest material in organic light-emitting diodes that exhibit NIR emission with the maximum external quantum efficiency (EQE_{max}) of 1.09% and the maximum radiance of 4042 mW Sr^{-1} m^{-2}.

Introduction

Kasha's rule[1] is extensively observed in luminescence fields,[2–4] such as in fluorescent molecular rotors,[3,5–8] bioimaging[9–13] and organic light-emitting diodes (OLEDs),[14–17] in which the excitons return to the ground state from the lowest singlet S_1 (for phosphorescence this process occurs from T_1). To date, most organic luminescent materials follow this rule and their photophysical properties can be precisely simulated using quantum chemical calculations. Recent work on fluorescent molecular rotors indicates that Kasha's rule could be sketchily suppressed by controlling the order of emissive states.[5] However, regarding these categories of compounds, some great challenges need to be addressed: (1) inapparent variation of emitting colors that bedims the discrimination, especially, with the naked eye;[5,18–21] (2) the deficiency of near-infrared (NIR) emission that limits the general applicability in bioluminescence fields;[9,20–25] and (3) an unclear mechanism that restricts the molecular design and applications, especially, from the aspect of the connection between the molecular configuration and the matrix.[18,19,22,26–33] Additionally, almost all studies focus on the transition from low to high excited states rather than the other way around, which cannot dialectically expose the nature of Kasha's rule.[5–9,20,21,23–25,34]

In a previous work, we reported a series of phenazine-based compounds[14] to explore the connection between the electronic configuration of the excited state and the molecular configuration. The results show that the emission of phenazine-based compounds could undergo a bathochromic-shift with the increase of electron-donating ability of the donor. However, among the phenazine-based family, phenoxazine–phenazine (POZ–PZ) exhibits unanticipated dual emission (~420 nm intense mazarine and 780 nm weak NIR) in the solution state and single NIR emission (~760 nm) in the thin film state (Fig. 1a). The visible chromatism range reaches up to ~340 nm. This huge chromatism means that two emissions might come

[a] *School of Chemistry and Chemical Engineering, Frontiers Science Center for Transformative Molecules, Shanghai Key La-boratory of Electrical Insulation and Thermal Aging, Shanghai Jiao Tong University, Shanghai 200240, China. E-mail: litao1983@sjtu.edu.cn*
[b] *Institute of Functional Nano & Soft Materials (FUNSOM) and Jiangsu Key Laboratory for Carbon-Based Functional Materi-als & Devices, Soochow University, Suzhou 215006, China. E-mail: dyzhou@suda.edu.cn*
[c] *Giant E-tech of State Development and Investment Corporation (SDIC), Jinan 250100, China*

† Electronic supplementary information (ESI) available: Methods and materials, details of photoreactions, electrical properties, and NMR and simulation results. See DOI: https://doi.org/10.1039/d3qm00394a

‡ These authors contributed equally to this work.

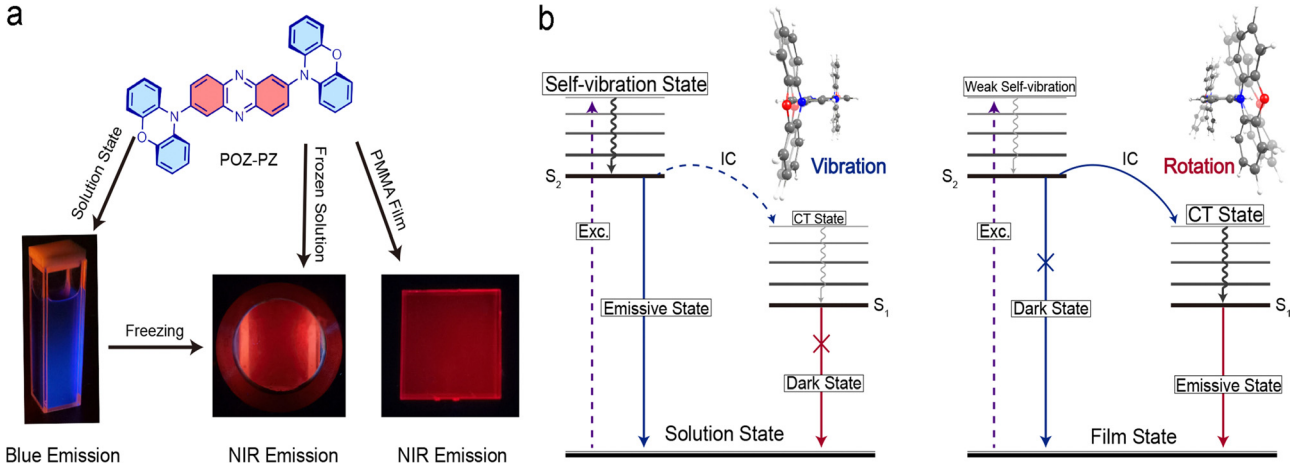

Fig. 1 (a) The molecular structure of POZ–PZ and images obtained under a 365 nm UV-lamp. The concentration of the solution state is 10^{-5} M in toluene and the film is doped with 10 wt% in PMMA. The frozen solution is obtained using the identical solution to freeze in the cryo-stat; (b) schematic diagrams of emissive mechanisms in different matrixes.

from the disparate energy levels rather than the localized excitation (LE) state and the charge transfer (CT) state of the unitary energy level (LE and CT of S_1).

Based on these phenomena, in this work, specific research has been conducted to try to reveal the mechanism for the variable emission. We propose that the blue emission in solution comes from the high-level excited state (S_n, $n \geq 2$), and the NIR emission is from the lowest excited state (S_1) (Fig. 1b). This hypothesis is well supported by the subsequent experimental and simulated results, proving that Kasha's rule can be suppressed in unrestrictive matrixes (low-viscosity solution) due to the vertical configuration between the donor (POZ) and the acceptor (PZ). It is also supported that the blue emission primarily comes from the self-vibration of the POZ group. Meanwhile, the single NIR emission in rigid matrixes (thin film, high-viscosity solution or PMMA) completely comes from the lowest singlet state, through the utilization of Kasha's rule. This matrix-induced Kasha's rule (MIKR) could be preferably used to expound the reason for variable emission of the objective molecule. Furthermore, POZ–PZ is also utilized as a guest material in OLED devices. The results demonstrate that the emitter could conform to Kasha's rule and the devices exhibit NIR emission with an EQE_{max} of 1.09% and a $radiance_{max}$ of 4042 mW Sr^{-1} m^{-2}.

Results and discussion

Design and synthesis

For the synthesis procedures please refer to the previous work[14] and supporting information. On the one hand, we previously found that the oscillator strength of S_1 approaches zero if the dihedral angle is vertical, which means S_1 may no longer be an ideal emissive state. Compared with common donors (such as carbazole (Cz), tertbutylcarbazole (*t*BCz) and so on), POZ has stronger electron-donating ability, while the flexible connection between two benzene rings of POZ could guarantee the vibration of groups around the N–O axis. In addition, POZ has a relatively larger dihedral angle with the acceptor than the above donors,[35–52] which also provides an advantage for realizing the vertical configuration of POZ–PZ in solution. Therefore, we prudently consider that POZ–PZ is an appropriate object to explore the connection between Kasha's rule and molecular configuration. On the other hand, the method of *reductio ad absurdum* is adopted to verify the accuracy of our consideration. A new analog, 2,6-bis(4,5-bis(diphenylphosphanyl)-10*H*-phenoxazin-10-yl)phenazine (DPh_2P-POZ–PZ), which has bulky groups (diphenylphosphine) on POZ is synthesized as a contrast compound to restrict the intramolecular motion, especially, most of the self-vibration and partial rotation.

Photophysical properties

As depicted in Fig. 2a, POZ–PZ has two distinct absorption bands around 533 (low-energy band) and 326 nm (high-energy band) in toluene solution. The former can be ascribed to the CT transition of S_1 and the latter can be attributed to a higher energy level. In contrast, the absorption in the thin film state exhibits noteworthy distinctions compared to the absorption in the solution state: the low-energy band shifts to 553 nm and the absorbance of the high-energy band experiences a substantial decrease and alteration, which can be ascribed to the alteration of the matrix. POZ–PZ shows two emission peaks in solution, which are around 420 and 780 nm. However, only one peak (760 nm) is observed in the thin film state. As mentioned above, we hypothesize that the emission peaks around 420 nm and 780 nm in the solution state might be attributed to S_2 and S_1, respectively. To prove this point, different excitation lamps are utilized to excite the emitter in solution. As shown in Fig. 2b, POZ–PZ presents two peaks under a 365 nm light source in the solution state. Meanwhile, a 550 nm lamp is carefully chosen to be a low-energy light source in order to keep away from the short-wavelength emitting peak. Obviously, the single NIR emission peak indicates that the long-wavelength peak indeed

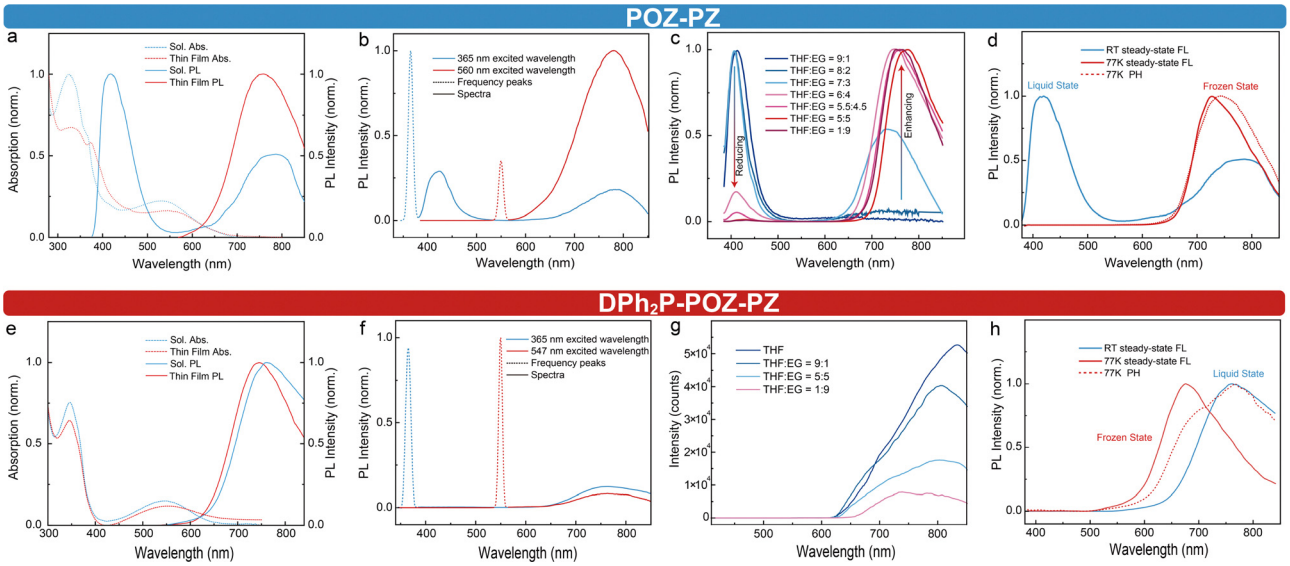

Fig. 2 (a and e) The absorption and PL spectra in toluene solution (10^{-5} M) and pure thin film; (b and f) the PL spectra under different excitation lamps. (c and g) The viscosity-dependent spectra tested at 20 °C, volume/volume for every set; (d and h) the steady-state FL (blue line) in toluene solution (10^{-5} M) at room temperature, the phosphorescence (red dash) and steady-state FL (red line) in frozen toluene solution (identical solution with RT steady-state FL) at 77 K.

comes from the S_1 and the insufficient excitation power cannot excite the blue emission, which demonstrates that the dual-emission process in solution belongs to different excited states rather than the LE state and CT state of S_1.[5]

To further explore the possible reasons for the disappearance of the short-wavelength peak in the thin film state, high-viscosity solvents are employed to restrict the molecular motion of POZ–PZ, which is aimed at gradually approximating to the circumstances of the thin film state. Taking into consideration of the solubility of POZ–PZ and the intermiscibility of different solvents, ethylene glycol (EG, high-viscosity) and tetrahydrofuran (THF, low-viscosity) are picked as mixed solution and measurements were carried out at 20 °C. As shown in Fig. 2c, viscosity-dependent spectra are normalized because of the weak emission in low-restrictive solution (low-viscosity solution). In this way, the respective variations of the two emission peaks can be compared by their proportional variations in the whole emission. Under low-viscosity conditions ($V_{THF}:V_{EG}$ = 9 : 1), an intense peak appears in the short-wavelength range. Due to the large dipole moment of POZ–PZ and the high polarity of mixture solvents, the long-wavelength peak is very weak (compared with the emission in toluene solution). However, the proportion of the short-wavelength peak decreases as the solvent viscosity increases, and meanwhile, the proportion of the long-wavelength peak increases rapidly. The short-wavelength peak almost completely disappears when the solvent mixture reaches the highest viscosity ($V_{THF}:V_{EG}$ = 1 : 9).

Based on the results obtained above, the possible reasons could be inferred as follows: (i) because of the vertical dihedral angle between POZ and PZ, the electronic transition from the donor to acceptor is forbidden (especially for the π–π* transition) and the excitons have to execute the deexcitation *via* the self-vibration of the POZ group; (ii) due to the intramolecular rotation, the POZ group would reciprocally twist with an extent of angle along the pair-bearing moieties (the C–N bond) between POZ and PZ; this results in the CT emission appearing in the long-wavelength range when the dihedral angle is not vertical. These possible reasons indicate that the self-vibration of POZ produces blue emission, while the rotation of POZ determines the generation of NIR emission. Both these intramolecular motions (self-vibration and rotation) simultaneously lead to the concomitant and competitive dual emission in the solution state. When the high-viscosity solution is employed, the self-vibration and intramolecular rotation are both restricted, while the dihedral angle between POZ and PZ is confined to a feasible angle ϕ ($90^\circ > \phi > 68.9^\circ$, for detailed discussions see the simulations section) and more electrons could effectively transfer from the donor to acceptor rather than participating in the self-vibration of POZ. When the extent of restriction reaches the rigid matrix conditions, for instance the thin film state, the blue emission completely disappears.

The self-vibration and rotation of POZ–PZ could also be further attested by the low-temperature spectra. As shown in Fig. 2d, the state of the toluene solvent transforms from the unrestrictive matrix to restrictive matrix when the temperature reaches the freezing point, while the self-vibration is restricted by the restrictive matrix and the blue emission disappears. The alternative matrix immediately induces the dihedral angle to reach a new degree, which results in the NIR emission showing a hypsochromic shift to 725 nm. The experimental results indicate that not only do the self-vibration and rotation exist in POZ–PZ, but Kasha's rule also can be tuned by controlling the self-vibration and rotation. This process is completely induced by the variations of the matrixes.

Similar experiments have been also conducted on DPh_2-P-POZ–PZ. As expected, DPh_2P-POZ–PZ only has one emission peak around 759 nm in toluene solution due to the restriction of bulky groups for the self-vibration of POZ (Fig. 2e). The single emission also reflects that the dihedral angle between DPh_2P-POZ and PZ is set at a feasible angle. Meanwhile, based on the nearly identical absorption spectra observed in different matrices, it can be inferred that DPh2P-POZ–PZ does not undergo rotation due to the bulky group. The solution photoluminescence (PL) spectra of DPh_2P-POZ–PZ with different viscosities are also measured for comparison (see Fig. 2g). The results indicate that, because of the deficiency of self-vibration for the DPh_2P-POZ group and doable electron transition between the donor and the acceptor resulting from the feasible dihedral angle (64°), there is no noticeable emission that arises in a short-wavelength range. The absence of blue emission for DPh_2P-POZ–PZ further provides evidence that the blue emission of POZ–PZ comes from the self-vibration of the POZ group.

The photoluminescence quantum yields (ϕ_{PLQY}) of POZ–PZ in toluene and the polymethyl methacrylate (PMMA) film are 1.50% and 84.57%, respectively, confirming that the intramolecular motions (especially for self-vibration of the POZ group) are sufficiently suppressed in PMMA.

Simulations

Density functional theory (DFT) and time-dependent density functional theory (TD-DFT) simulations are employed at the B3LYP/6-31G** level to further verify our hypothesis. Firstly, the molecular configuration of the ground state has been optimized in a toluene atmosphere and the whole optimization processes are not restrictive. As shown in Fig. 3c, the dihedral angle between PZ and POZ is 90°, which agrees well with the hypothesis. As mentioned above, the short-wavelength peak disappears in the film state, which means that the self-vibration of POZ is forcefully weakened and the electrons could efficiently transfer from the POZ to PZ group profiting from the feasible dihedral angle, while the energy of the molecule is at the lowest point and the molecule is at the relatively stable state. Therefore, we scanned the potential energy of the POZ–PZ molecule to simulate the feasible dihedral angle between the POZ and PZ groups. Fig. 3a shows a three-dimensional diagram of the angle-dependent potential energy. ϕ_1 is the dihedral angle of one POZ group with PZ, and ϕ_2 is the other one. It clearly demonstrates that when ϕ_1 and ϕ_2 are both ~68.9°, the molecule has the lowest energy. At this stage, this structure is picked up for further optimization and finally is deemed as the feasible configuration in the film state. After obtaining the optimized configurations in different matrixes, TD-DFT is employed to evaluate the properties of excited states. It is worth noting that TD-DFT is based on the Born–Oppenheimer approximation; however, the blue emission of S_2 results from the intramolecular motion that is at least four orders of magnitude faster than the rate of the emissive state (S_1). Therefore, the surface of S_2 is for quantitative reference only. The detailed discussion is provided alongside Fig. S4 (ESI†). We

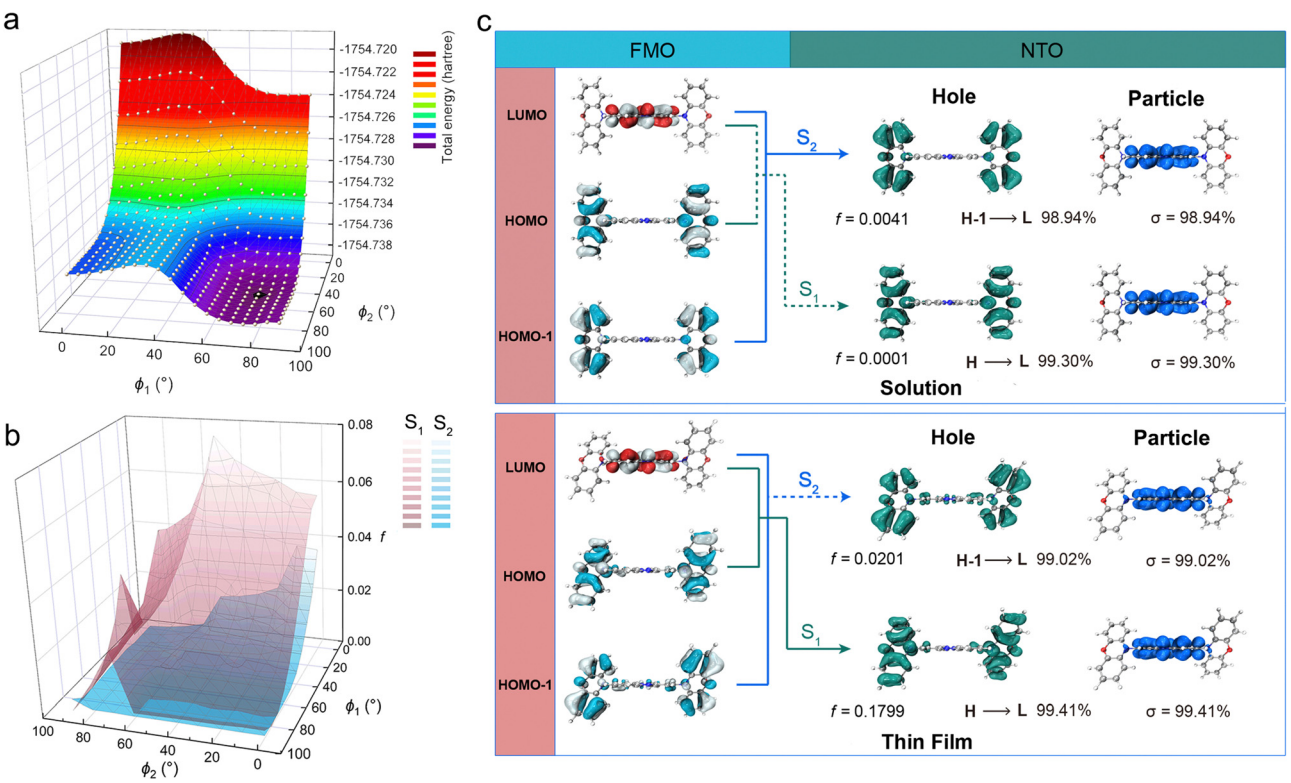

Fig. 3 (a) The potential energy scanning of angle-dependence of POZ–PZ; (b) the oscillator strength of the excited state for angle-dependence of POZ–PZ; and (c) the surfaces of frontier molecular orbitals (sky-blue and claret-red) and natural transition orbitals (turquoise and mazarine).

present the surfaces of S_1 and S_2 states in Fig. 3c. In the solution state, the oscillator strength (f) of S_1 exhibits a negligible value of 0.0001 and the excitation energy is 1.51 eV, corresponding to 788 nm. The oscillator strength of S_2 is up to 0.0041, and the excitation energy is 2.99 eV, which corresponds to 414 nm. These simulated wavelengths are consistent with the emission spectra in solution. Turning to the excited state of a feasible structure in the film, the results show that the oscillator strength of S_1 is 0.1799. Contrarily, the oscillator strength of S_2 is merely 0.0201. When compared to S_2, S_1 is a viable emissive state for this molecular configuration. Meanwhile, the excitation energy of S_1 is 1.63 eV, corresponding to 763 nm, which matches well with the PL spectrum in the thin film state. To further visually probe the connection between the dihedral angle and oscillator strength, the angle-dependent oscillator strength under the scan pattern is calculated. As shown in Fig. 3b, the oscillator strength of S_1 is prominently larger than that of S_2 with a small dihedral angle. As the dihedral angle increases, both oscillator strengths (S_1 and S_2) decrease rapidly, which is due to the increasing difficulty of electron-transition from POZ to PZ. The electron transition of S_1 is almost forbidden when the dihedral angle is 90°, which means that the oscillator strength of S_1 approaches zero and it is lower than that of S_2. Therefore, Kasha's rule is suppressed and the emission would be generated from S_2. Importantly, these simulation results agree well with the experimental results and provide persuasive evidence for our hypothesis. At the same time, the level of involvement for the acceptor, crucial to the phenazine system, would directly impact the performance in the excited state. The vibration vector is analysed to qualitatively illustrate the degree of involvement of the acceptor (detailed discussion is given in Fig. S3, ESI†).

Combining the experimental and the simulation results, our hypothesis can be confirmed: (i) in the solution state, due to the absence of a restrictive matrix, the POZ group tends to be vertical to the PZ group. This vertical configuration results in an ineffective electronic transition between POZ and PZ, and thus, the excitons de-excite through the non-radiative transition and self-vibration emission paths. This agrees well with the extremely low ϕ_{PLQY} and blue emission in the solution state; (ii) contrarily, in the thin film state, the vibration and rotation of the POZ group are to some extent restricted by the stacking interaction. Meanwhile, the dihedral angle is maintained at a feasible angle. Benefiting from these points, the high ϕ_{PLQY} and the single emission peak signify that the electrons originally aggregated at the POZ group can transfer to the PZ group and undergo CT-type transition, and the S_1 transforms into an emissive state. By harnessing this mechanism, the photophysical properties can be adjusted through the choice of matrix. For example, employing different polymers enables tunable emission to be achieved (Fig. S20, ESI†).

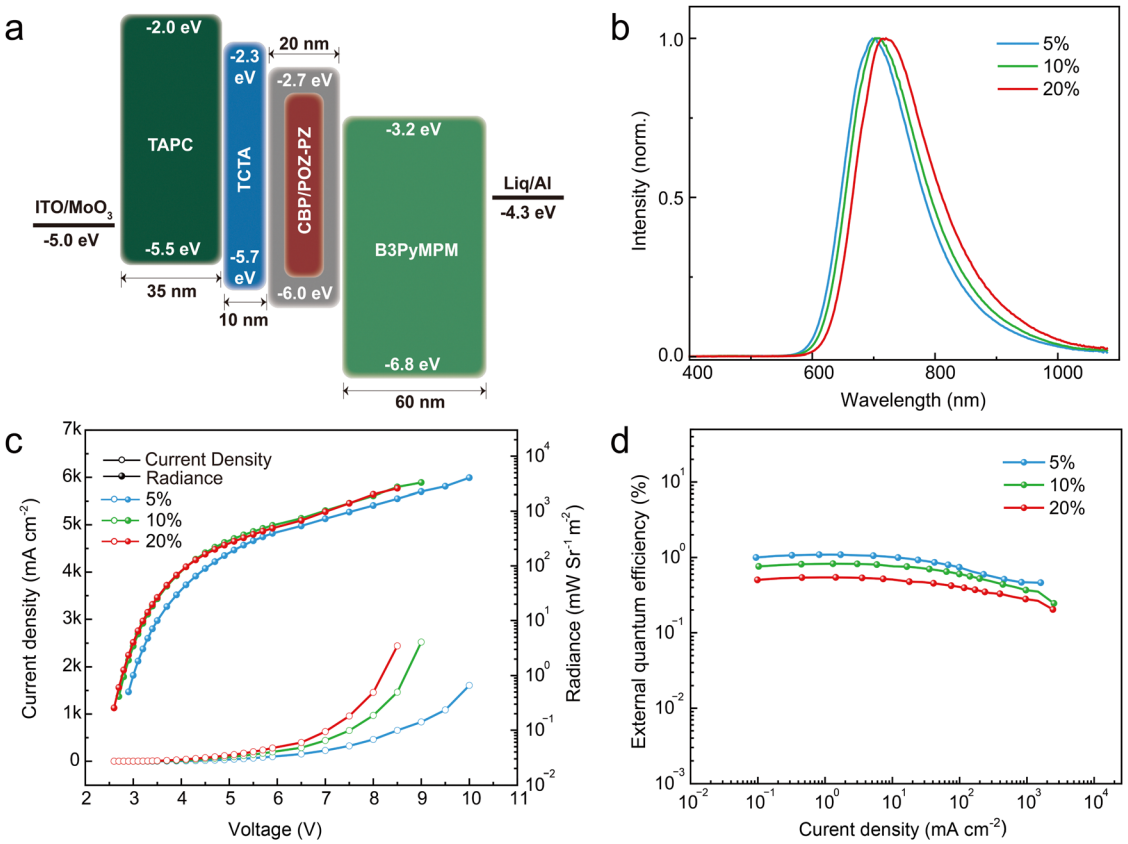

Fig. 4 (a) The architecture of devices; (b) the electroluminescence spectra of POZ–PZ; (c) the voltage–current density–radiance curves for POZ–PZ; and (d) the current-density–EQE curves for POZ–PZ.

Electroluminescence properties

After exploring the photophysical properties, OLED devices were fabricated with a confirmatory architecture (Fig. 4a) to further explore the electroluminescence properties of POZ–PZ: indium tin oxide (ITO)/molybdenum trioxide (MoO_3) (1 nm)/4,4′-cyclohexylidenebis[*N*,*N*-bis(4-methylphenyl)aniline] (TAPC) (35 nm)/tris(4-(9H-carbazol-9-yl) phenyl)amine (TCTA) (10 nm)/CBP: *x* wt% POZ–PZ (20 nm)/4,6-bis(3,5-di-3-pyridylphenyl)-2-methylpyrimidine (B3PYMPM) (60 nm)/8-hydroxyquinolato-lithium (Liq) (2 nm)/Al (120 nm). TCTA and CBP are utilized as the exciton blocking layer and the host material, respectively. MoO_3 and Liq are selected as the hole injection layer and the electron injection layer, respectively. TAPC and B3PYMPM are used as the hole transporting layer and the electron transporting layer, respectively. Before measuring the electroluminescence properties, we also prepared a POZ–PZ doped PMMA film (10 wt%) to measure the emission wavelength of unimolecules (Fig. S9, ESI†). The PL spectrum of the doped PMMA film shows that the emission peak is at around 715 nm (Fig. 1a). Compared with the pure thin film, the blue shift of the PMMA doped film is attributed to the absence of molecular aggregation, and this phenomenon also reflects in OLED devices with different doping concentrations. On this basis, three doping concentrations (5%, 10% and 20%) are selected for the fabrication of the devices. As shown in Fig. 4b, the EL peaks are at 702, 708 and 720 nm for 5%, 10% and 20% concentrations, respectively, and the bulk of the EL spectra falls in the NIR range. As mentioned above, the aggregation of molecules makes a difference to the emission wavelength. The 5%, 10% and 20% concentration devices exhibit the EQE_{max} values of 1.09%, 0.83% and 0.54%, respectively. The maximum radiance values are 4042, 3301 and 2596 mW Sr^{-1} m^{-2} for the 5%, 10% and 20% doped devices, respectively. The EQEs of $radiance_{max}$ are maintained at 0.46%, 0.24% and 0.20% for the 5%, 10% and 20% doped devices, respectively. These roll-offs of EQEs are ascribed to the intense collision-induced quenching effects during the EL process. Naturally, the non-radiative transition of the molecule resulted from the vibration, and rotation is also a nonnegligible reason despite that these non-radiative transitions are partially restricted by the doped film state. However, according to the radiance, fair efficiency and NIR emission, POZ–PZ is expected to be a promising OLED guest material.

Conclusions and outlook

In this paper, we elaborately studied an unusual phenomenon of phenazine-based compound POZ–PZ. In the solution state, POZ–PZ exhibits blue emission and NIR emission by suppressing Kasha's rule. Based on the experimental analyses and the method of *reductio ad absurdum*, the blue emission can be attributed to the self-vibration of the POZ group, which comes from the vertical configuration between the donor and acceptor. At the same time, the viscosity-dependent analyses and PL spectra sufficiently prove that POZ and PZ could rotate to a feasible angle (68.9°) in restrictive matrixes to make the charge transfer efficient, further forming a single NIR emission by utilizing Kasha's rule. Such large variations in emission (visible chromatism reaches up to ~340 nm) in different matrixes could be clearly discriminated by the naked eye, which is rare in congeneric materials, and this emission-variation phenomenon that transforms from anti-Kasha's rule to obeying Kasha's rule is scarcely addressed in previous works. Meanwhile, the results of simulations have clearly shown the connection between the molecular configuration and Kasha's rule at the molecular self-consistency state.[53] Therefore, based on the experimental and simulated results, a matrix-induced Kasha's rule (MIKR) mechanism is proposed, where the matrixes would influence the molecular configuration and intramolecular motion, further affecting the photophysical properties of the molecules. This viewpoint has never been deeply explored before this work. OLED devices are also fabricated to verify the electroluminescence properties of POZ–PZ. The results show that EQE_{max} reaches 1.09%, and a $radiance_{max}$ value of 4042 mW Sr^{-1} m^{-2} can be achieved, while the emissive peak is over 702 nm, exhibiting NIR emission. We believe that this specific MIKR mechanism based on POZ–PZ could contribute new strategies for molecular design and a deep understanding of photophysics.

Author contributions

M. Xie and J.-H. Cai performed all the syntheses and spectroscopic and computational characterization. G. Zhang performed the TGA and DSC analyses. S. Jung, Z.-Y. Zhang and D. Dong performed the kinetic investigations. D.-Y. Zhou, L.-S. Liao and T. Li supervised the research activities. All authors contributed to the final version of the manuscript.

Conflicts of interest

The authors declare no competing financial interest.

Acknowledgements

The authors acknowledge financial support from the National Natural Science Foundation of China (22022507, 51973111, and 22209110), the Natural Science Foundation of Jiangsu Province (BK20221237), China Scholarship Council (202206230152), Open Foundation of Shanghai Jiao Tong University Shaoxing Research Institute of Renewable Energy and Engineering (JDSX2022057) and China Postdoctoral Science Foundation (2020M681279).

Notes and references

1 M. Kasha, Characterization of electronic transitions in complex molecules, *Discuss. Faraday Soc.*, 1950, **9**, 14–19.
2 G. Vaccaro, A. Bianchi, M. Mauri, S. Bonetti, F. Meinardi, A. Sanguineti, R. Simonutti and L. Beverina, Direct monitoring of self-assembly of copolymeric micelles by a

luminescent molecular rotor, *Chem. Commun.*, 2013, **49**, 8474–8476.
3 Y. Shiraishi, T. Inoue and T. Hirai, Local viscosity analysis of triblock copolymer micelle with cyanine dyes as a fluorescent probe, *Langmuir*, 2010, **26**, 17505–17512.
4 Q. J. Meisner, A. H. Younes, Z. Yuan, K. Sreenath, J. J. M. Hurley and L. Zhu, Excitation-Dependent Multiple Fluorescence of a Substituted 2-(2′-Hydroxyphenyl)benzoxazole, *J. Phys. Chem. A*, 2018, **122**, 9209–9223.
5 H. Qian, M. E. Cousins, E. H. Horak, A. Wakefield, M. D. Liptak and I. Aprahamian, Suppression of Kasha's rule as a mechanism for fluorescent molecular rotors and aggregation-induced emission, *Nat. Chem.*, 2017, **9**, 83–87.
6 J. Dong, K. Zhang, X. Li, Y. Qian, H. Zhu, D. Yuan, Q. H. Xu, J. Jiang and D. Zhao, Ultrathin two-dimensional porous organic nanosheets with molecular rotors for chemical sensing, *Nat. Commun.*, 2017, **8**, 1142.
7 J. Zhang, A. Rakhimbekova, X. Duan, Q. Yin, C. A. Foss, Y. Fan, Y. Xu, X. Li, X. Cai, Z. Kutil, P. Wang, Z. Yang, N. Zhang, M. G. Pomper, Y. Wang, C. Barinka and X. Yang, A prostate-specific membrane antigen activated molecular rotor for real-time fluorescence imaging, *Nat. Commun.*, 2021, **12**, 5460.
8 M. K. Kuimova, S. W. Botchway, A. W. Parker, M. Balaz, H. A. Collins, H. L. Anderson, K. Suhling and P. R. Ogilby, Imaging intracellular viscosity of a single cell during photoinduced cell death, *Nat. Chem.*, 2009, **1**, 69–73.
9 M. Ibarra-Rodri Guez, B. M. Munoz-Flores, H. V. Dias, M. Sanchez, A. Gomez-Trevino, R. Santillan, N. Farfan and V. M. Jimenez-Perez, Fluorescent Molecular Rotors of Organoboron Compounds from Schiff Bases: Synthesis, Viscosity, Reversible Thermochromism, Cytotoxicity, and Bioimaging Cells, *J. Org. Chem.*, 2017, **82**, 2375–2385.
10 K. Zhang, F. Yang, Y. Zhang, Y. Ma, J. Fan, J. Fan, C. K. Wang and L. Lin, Highly Efficient Near-Infrared Thermally Activated Delayed Fluorescence Molecules via Acceptor Tuning: Theoretical Molecular Design and Experimental Verification, *J. Phys. Chem. Lett.*, 2021, **12**, 1893–1903.
11 C. Dragonetti, F. Fagnani, D. Marinotto, A. di Biase, D. Roberto, M. Cocchi, S. Fantacci and A. Colombo, First member of an appealing class of cyclometalated 1,3-di-(2-pyridyl)benzene platinum(ii) complexes for solution-processable OLEDs, *J. Mater. Chem. C*, 2020, **8**, 7873–7881.
12 J. Wang, X. Gu, H. Ma, Q. Peng, X. Huang, X. Zheng, S. H. P. Sung, G. Shan, J. W. Y. Lam, Z. Shuai and B. Z. Tang, A facile strategy for realizing room temperature phosphorescence and single molecule white light emission, *Nat. Commun.*, 2018, **9**, 2963.
13 Z. An, C. Zheng, Y. Tao, R. Chen, H. Shi, T. Chen, Z. Wang, H. Li, R. Deng, X. Liu and W. Huang, Stabilizing triplet excited states for ultralong organic phosphorescence, *Nat. Mater.*, 2015, **14**, 685–690.
14 M. Xie, J. Cai, X. Wang, T. Shan, S. Jung, H. Zhong, X. Guo, D. Zhou and T. Li, Simple Phenazine-Based Compounds Realizing Superior Multicolored Emission, *Adv. Opt. Mater.*, 2022, **10**, 2102443.
15 M. Xie, C. Han, Q. Liang, J. Zhang, G. Xie and H. Xu, Highly efficient sky blue electroluminescence from ligand-activated copper iodide clusters: Overcoming the limitations of cluster light-emitting diodes, *Sci. Adv.*, 2019, **5**, eaav9857.
16 Y. Xu, P. Xu, D. Hu and Y. Ma, Recent progress in hot exciton materials for organic light-emitting diodes, *Chem. Soc. Reviews*, 2021, **50**, 1030–1069.
17 L. Qin, W. Ma, M. Hanif, J. Jiang, Z. Xie and Y. Ma, Donor–Node–Acceptor Polymer with Excellent n-Doped State for High-Performance Ambipolar Flexible Supercapacitors, *Macromolecules*, 2017, **50**, 3565–3572.
18 J. Dong, Y. Pan, H. Wang, K. Yang, L. Liu, Z. Qiao, Y. D. Yuan, S. B. Peh, J. Zhang, L. Shi, H. Liang, Y. Han, X. Li, J. Jiang, B. Liu and D. Zhao, Self-Assembly of Highly Stable Zirconium(IV) Coordination Cages with Aggregation Induced Emission Molecular Rotors for Live-Cell Imaging, *Angew. Chem., Int. Ed.*, 2020, **59**, 10151–10159.
19 L. J. Patalag, J. Hoche, R. Mitric, D. B. Werz and B. L. Feringa, Transforming Dyes into Fluorophores: Exciton-Induced Emission with Chain-like Oligo-BODIPY Superstructures, *Angew. Chem., Int. Ed.*, 2022, **61**, e202116834.
20 C. Wang, T. Wang, M. Zhao, F. Dai, Z. Niu, W. Zhang and Y. Ma, A simple chalcone molecular rotor for specific fluorescence imaging of mitochondrial viscosity changes in living cells, *Dyes and Pigm.*, 2021, **194**, 109593.
21 K. Cao, M. Farahi, M. Dakanali, W. M. Chang, C. J. Sigurdson, E. A. Theodorakis and J. Yang, Aminonaphthalene 2-cyanoacrylate (ANCA) probes fluorescently discriminate between amyloid-beta and prion plaques in brain, *J. Am. Chem. Soc.*, 2012, **134**, 17338–17341.
22 T. Suhina, D. Bonn, B. Weber and A. M. Brouwer, Photophysics of Fluorescent Contact Sensors Based on the Dicyanodihydrofuran Motif, *Chem. Phys. Chem.*, 2021, **22**, 221–227.
23 A. Vyšniauskas and M. K. Kuimova, A twisted tale: measuring viscosity and temperature of microenvironments using molecular rotors, *Intern. Rev. Phys. Chem.*, 2018, **37**, 259–285.
24 J. Sturala, M. K. Etherington, A. N. Bismillah, H. F. Higginbotham, W. Trewby, J. A. Aguilar, E. H. C. Bromley, A. J. Avestro, A. P. Monkman and P. R. McGonigal, Excited-State Aromatic Interactions in the Aggregation-Induced Emission of Molecular Rotors, *J. Am. Chem. Soc.*, 2017, **139**, 17882–17889.
25 L. Wang, Y. Xiao, W. Tian and L. Deng, Activatable rotor for quantifying lysosomal viscosity in living cells, *J. Am. Chem. Soc.*, 2013, **135**, 2903–2906.
26 Y. Cheng, J. Wang, Z. Qiu, X. Zheng, N. L. C. Leung, J. W. Y. Lam and B. Z. Tang, Multiscale Humidity Visualization by Environmentally Sensitive Fluorescent Molecular Rotors, *Adv. Mater.*, 2017, **29**, 1703900.
27 J. Bao, R. Lan, C. Shen, R. Huang, Z. Wang, W. Hu, L. Zhang and H. Yang, Modulation of Chirality and Intensity of Circularly Polarized Luminescence Emitting from Cholesteric Liquid Crystals Triggered by Photoresponsive Molecular Motor, *Adv. Opt. Mater.*, 2021, **10**, 2101910.

28 D. Dziuba, P. Jurkiewicz, M. Cebecauer, M. Hof and M. Hocek, A Rotational BODIPY Nucleotide: An Environment-Sensitive Fluorescence-Lifetime Probe for DNA Interactions and Applications in Live-Cell Microscopy, *Angew. Chem., Int. Ed.*, 2016, **55**, 174–178.

29 Y. Shi, H. Guo, J. Huang, X. Zhang, Z. Wu, K. Yang, Y. Zhang, K. Feng, H. Y. Woo, R. P. Ortiz, M. Zhou and X. Guo, Distannylated Bithiophene Imide: Enabling High-Performance n-Type Polymer Semiconductors with an Acceptor-Acceptor Backbone, *Angew. Chem., Int. Ed.*, 2020, **59**, 14449–14457.

30 S. G. Srivatsan, N. J. Greco and Y. Tor, A highly emissive fluorescent nucleoside that signals the activity of toxic ribosome-inactivating proteins, *Angew. Chem., Int. Ed.*, 2008, **47**, 6661–6665.

31 L. Feng, Y. Xie, S. K. Au-Yeung, H. B. Hailu, Z. Liu, Q. Chen, J. Zhang, Q. Pang, X. Yao, M. Yang, L. Zhang and H. Sun, A fluorescent molecular rotor probe for tracking plasma membranes and exosomes in living cells, *Chem. Commun.*, 2020, **56**, 8480–8483.

32 J. Zhang, H. Zhang, J. W. Y. Lam and B. Z. Tang, Restriction of Intramolecular Motion(RIM): Investigating AIE Mechanism from Experimental and Theoretical Studies, *Chem. Res. Chin. Univ.*, 2021, **37**, 1–15.

33 S. C. Lee, C. L. Lee, J. Heo, C. U. Jeong, G. H. Lee, S. Kim, W. Yoon, H. Yun, S. O. Park, S. K. Kwak, S. H. Park and O. P. Kwon, Molecular Viscosity Sensors with Two Rotators for Optimizing the Fluorescence Intensity-Contrast Trade-Off, *Chemistry*, 2018, **24**, 2888–2897.

34 J. C. del Valle and J. Catalán, Kasha's rule: a reappraisal, *Phys. Chem. Chem. Phys.*, 2019, **21**, 10061–10069.

35 K. Wu, T. Zhang, Z. Wang, L. Wang, L. Zhan, S. Gong, C. Zhong, Z. H. Lu, S. Zhang and C. Yang, De Novo Design of Excited-State Intramolecular Proton Transfer Emitters via a Thermally Activated Delayed Fluorescence Channel, *J. Am. Chem. Soc.*, 2018, **140**, 8877–8886.

36 J. H. Kim, J. H. Yun and J. Y. Lee, Recent Progress of Highly Efficient Red and Near-Infrared Thermally Activated Delayed Fluorescent Emitters, *Adv. Opt. Mater.*, 2018, **6**, 1800255.

37 J. X. Chen, W. W. Tao, W. C. Chen, Y. F. Xiao, K. Wang, C. Cao, J. Yu, S. Li, F. X. Geng, C. Adachi, C. S. Lee and X. H. Zhang, Red/Near-Infrared Thermally Activated Delayed Fluorescence OLEDs with Near 100% Internal Quantum Efficiency, *Angew. Chem., Int. Ed.*, 2019, **58**, 14660–14665.

38 Z. Wu, Y. Liu, L. Yu, C. Zhao, D. Yang, X. Qiao, J. Chen, C. Yang, H. Kleemann, K. Leo and D. Ma, Strategic-tuning of radiative excitons for efficient and stable fluorescent white organic light-emitting diodes, *Nat. Commun.*, 2019, **10**, 2380.

39 D. Zhang, X. Song, H. Li, M. Cai, Z. Bin, T. Huang and L. Duan, High-Performance Fluorescent Organic Light-Emitting Diodes Utilizing an Asymmetric Anthracene Derivative as an Electron-Transporting Material, *Adv. Mater.*, 2018, **30**, e1707590.

40 D. Zhang, X. Song, M. Cai and L. Duan, Blocking Energy-Loss Pathways for Ideal Fluorescent Organic Light-Emitting Diodes with Thermally Activated Delayed Fluorescent Sensitizers, *Adv. Mater.*, 2018, **30**, 1705250.

41 B. G. McCarthy, R. M. Pearson, C. H. Lim, S. M. Sartor, N. H. Damrauer and G. M. Miyake, Structure-Property Relationships for Tailoring Phenoxazines as Reducing Photoredox Catalysts, *J. Am. Chem. Soc.*, 2018, **140**, 5088–5101.

42 P. Heimel, A. Mondal, F. May, W. Kowalsky, C. Lennartz, D. Andrienko and R. Lovrincic, Unicolored phosphor-sensitized fluorescence for efficient and stable blue OLEDs, *Nat. Commun.*, 2018, **9**, 4990.

43 J. Guo, Z. Zhao and B. Z. Tang, Purely Organic Materials with Aggregation-Induced Delayed Fluorescence for Efficient Nondoped OLEDs, *Adv. Opt. Mater.*, 2018, **6**, 1800264.

44 T. T. Bui, F. Goubard, M. Ibrahim-Ouali, D. Gigmes and F. Dumur, Recent advances on organic blue thermally activated delayed fluorescence (TADF) emitters for organic light-emitting diodes (OLEDs), *Beilstein J. Org. Chem.*, 2018, **14**, 282–308.

45 Z. Yang, Z. Mao, Z. Xie, Y. Zhang, S. Liu, J. Zhao, J. Xu, Z. Chi and M. P. Aldred, Recent advances in organic thermally activated delayed fluorescence materials, *Chem. Soc. Rev.*, 2017, **46**, 915–1016.

46 P. K. Samanta, D. Kim, V. Coropceanu and J. L. Bredas, Up-Conversion Intersystem Crossing Rates in Organic Emitters for Thermally Activated Delayed Fluorescence: Impact of the Nature of Singlet *vs.* Triplet Excited States, *J. Am. Chem. Soc.*, 2017, **139**, 4042–4051.

47 X. C. Fan, K. Wang, Y. Z. Shi, D. M. Sun, J. X. Chen, F. Huang, H. Wang, J. Yu, C. S. Lee and X. H. Zhang, Thermally activated delayed fluorescence materials for non-doped organic light-emitting diodes with nearly 100% exciton harvest, *SmartMat*, 2023, **4**, e1122.

48 J. Huang, H. Nie, J. Zeng, Z. Zhuang, S. Gan, Y. Cai, J. Guo, S. J. Su, Z. Zhao and B. Z. Tang, Highly Efficient Nondoped OLEDs with Negligible Efficiency Roll-Off Fabricated from Aggregation-Induced Delayed Fluorescence Luminogens, *Angew. Chem., Int. Ed.*, 2017, **56**, 12971–12976.

49 K. Wu, T. Zhang, L. Zhan, C. Zhong, S. Gong, Z. H. Lu and C. Yang, Tailoring Optoelectronic Properties of Phenanthroline-Based Thermally Activated Delayed Fluorescence Emitters through Isomer Engineering, *Adv. Opt. Mater.*, 2016, **4**, 1558–1566.

50 C. Wang, X. Li, Y. Pan, S. Zhang, L. Yao, Q. Bai, W. Li, P. Lu, B. Yang, S. Su and Y. Ma, Highly Efficient Nondoped Green Organic Light-Emitting Diodes with Combination of High Photoluminescence and High Exciton Utilization, *ACS Appl. Mater. Inter.*, 2016, **8**, 3041–3049.

51 R. Noriega, E. S. Barnard, B. Ursprung, B. L. Cotts, S. B. Penwell, P. J. Schuck and N. S. Ginsberg, Uncovering Single-Molecule Photophysical Heterogeneity of Bright, Thermally Activated Delayed Fluorescence Emitters Dispersed in Glassy Hosts, *J. Am. Chem. Soc.*, 2016, **138**, 13551–13560.

52 L. Tu, Y. Xie, Z. Li and B. Tang, Aggregation-induced emission: Red and near-infrared organic light-emitting diodes, *SmartMat.*, 2021, **2**, 326–346.

53 M. J. Frisch, J. A. Pople and J. S. Binkley, Self-consistent molecular orbital methods 25. Supplementary functions for Gaussian basis sets, *J. Chem. Phys.*, 1984, **80**, 3265–3269.